The Effect of Dispersion Correction on the Adsorption of CO on Metallic Nanoparticles

Davis, Jack B. A.; Baletto, Francesca; Johnston, Roy L.

[Link to publication on Research at Birmingham portal](#)

Article

The Effect of Dispersion Correction on the Adsorption of CO on Metallic Nanoparticles

Jack B. A. Davis,[†] Francesca Baletto,[‡] and Roy L. Johnston*,[†]

[†]School of Chemistry, University of Birmingham, Birmingham, West Midlands B15 2TT, United Kingdom
[‡]Department of Physics, Kings College London, London WC2R 2LS, United Kingdom

ABSTRACT: The effect of dispersion corrections at a range of theory levels on the chemisorption properties of metallic nanoparticles is presented. The site preference for CO on Pt, Au, Pd, and Ir nanoparticles is determined for two geometries, the 38-atom truncated octahedron and the 55-atom icosahedron using density functional theory (DFT). The effects of Grimme's DFT-D2 and DFT-D3 corrections and the optPBE vdW-DF on the site preference of CO is then compared to the "standard" DFT results. Functional behavior is shown to depend not only on the metal but also on the geometry of the nanoparticle with significant effects seen for Pt and Au. There are both qualitative and quantitative differences between the functionals, with significant energetic differences in the chemical ordering of inequivalent sites and adsorption energies varying by up to 1.6 eV.
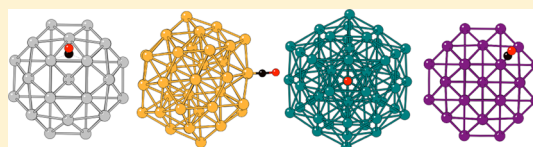
INTRODUCTION

Kohn−Sham density functional theory (DFT)[1,2] is widely used for the study of small molecule adsorption on metallic surfaces and nanoparticles (NPs). Although in most cases accurate, DFT requires the approximation of electron−electron interactions by exchange-correlation (xc) functionals. These often fail to describe the dispersion component of the van der Waals (vdW) energies, which arise from the response of electrons to instantaneous charge density fluctuations.

The consideration of dispersion energies in DFT is important in order to improve its overall chemical accuracy. Several methods exist for the consideration of dispersion, these include the Grimme DFT+D semiempirical approaches,[3−5] vdW density functionals (vdW-DF),[6−9] and higher-level methodologies, such as RPA.[10,11]

Methods for the inclusion of dispersion correction in DFT have been previously classified as a "stairway to heaven" with each step representing both increased accuracy and cost.[12] The first step is the addition of a pairwise energy term, calculated using precomputed dispersion coefficients that account for the missing interactions. This approach has a very low computational cost and is widely used but neglects many-body terms.[13] Coefficients are also kept constant, which causes such an approach to neglect any effects originating from an atom's environment. The second step, therefore, is the inclusion of environment-dependent coefficients. There are several approaches available, which include Grimme's DFT+D3,[5] Tkatchenko and Scheffler's vdW(TS),[14] and the Becke−Johnson model.[15] The third step on the "stairway" are vdW-DF's that obtain dispersion interactions directly from the electron density. These include vdW-DF and vdW-DF2[6,7] and Michaelides' optPBE.[9] These three "steps" will be investigated in the current work using Grimme's DFT-D2 and DFT-D3 and the optPBE vdW-DF.[3,5,9] Higher accuracy methods are available but these are limited to smaller system sizes.

Although not previously investigated for metallic nanoparticles, the effect of dispersion correction on the adsorption of small molecules on a variety of metal surfaces has been widely studied.[16−19] Previous DFT-GGA studies have been shown to be unable to replicate the experimental results of CO adsorption on Pt(111) surfaces.[20] It has been shown experimentally that the atop site is preferred, whereas GGA-DFT finds the hollow. Several approaches have been tested in order to solve this "puzzle", such as the use of other GGA and hybrid functionals.[21,22] These have proven to be inconclusive, as in the attempt to better describe the surface properties, nonlocal exchange causes the hybrid BLYP and B3LYP functionals to fail in accurately describing the bulk properties of the metal and also overestimate adsorption energies. More recently, the inclusion of the revPBE vdW-DF has shown some slight improvement in reproducing the relative energies between atop and hollow sites.[6,23]

Because of the relationship between metal NPs and bulk metals, it is hoped that the inclusion of dispersion will enable more accurate predictions of the site preferences for small molecules. In this study, we investigate the effect of dispersion correction on the chemisorption of CO on Pt, Au, Pd, and Ir NPs, all of which have been studied previously both theoretically and experimentally.[24−28] We opt for the study of the chemisorption of CO, a key contaminant of fuel cell catalysts, where CO acts as a poison on the Pt-anodes decreasing their lifetime and efficiency. For each metal, the magic-number 38-atom truncated octahedron (TO) and 55-atom icosahedron (Ico) are considered to investigate whether the effect of the corrections differs depending on the geometry of the cluster.

■ METHODOLOGY

DFT. Γ-point, spin-polarized calculations were performed with VASP,[29−32] using PAW pseudopotentials and a cutoff of 400 eV. Methfessel−Paxton smearing with a sigma value of 0.01 eV was used to improve metallic convergence.[33] The thresholds for the electronic energy and forces were set to 10^{-4} eV and 10^{-3} eV/Å, respectively.

The xc-functional was treated differently depending on the method of vdW correction. For the standard DFT and DFT +D2/3 methods, the PBE xc-functional was used,[34] whereas xc was explicitly treated by the optPBE functional.[8,9]

DFT+D2/3. Using Grimme's DFT+D2 approach,[3] the total energy is described by a sum of the Kohn−Sham energy, E_{DFT} and vdW semiempirical pair correction, $E_{disp}^{(2)}$

$$E_{DFT-D} = E_{KS-DFT} + E_{disp}^{(2)} \qquad (1)$$

$E_{disp}^{(2)}$ is given by

$$E_{disp}^{(2)} = -s_6 \sum_{i=1}^{N_{at-1}} \sum_{j=i+1}^{N_{at}} \frac{C_{ij}^6}{R_{ij}^6} f_{dmp}(R_{ij}) \qquad (2)$$

where N_{at} is the total number of atoms, C_{ij}^6 is the dispersion coefficient, R_{ij} is the bond distance for atom pair ij, and s_6 is a scaling factor, dependent on the xc-functional. A damping factor, f_{dmp}, is used to prevent singularities at small distances.

The DFT+D3 approach seeks to improve on the accuracy of DFT+D2 through the use of environment dependent dispersion coefficients during the DFT calculations and the inclusion of a three-body component to the E_{disp} term,

$$E_{disp} = E_{disp}^{(2)} + E_{disp}^{(3)} \qquad (3)$$

where $E_{disp}^{(3)}$ is given by

$$E_{disp}^{(3)} = \sum_{ABC} f_{f(3)}(\bar{r}_{ABC}) E^{ABC} \qquad (4)$$

and the sum is over all triples ABC. Geometrically averaged radii r^{-ABC} are used in the damping function, $f_{f(3)}$. The inclusion of three-body terms increases the scaling of the computational cost from $O(N_{atoms}^2)$ to $O(N_{atoms}^3)$, however, the cost of the inclusion of the D3 correction is still negligible when compared to the overall cost of a DFT calculation.

optPBE. The optPBE functional is an example of the vdW-DF approach,[6−9] which requires no external input and instead seeks to treat dispersion interactions directly using the electron density. The xc-energy is given by

$$E_{xc} = E_x^{GGA} + E_c^{LDA} + E_c^{nl} \qquad (5)$$

where E_x^{GGA} is the exchange energy for a given GGA functional and E_c^{LDA} is the LDA correlation energy. Dispersion is included directly using a nonlocal correlation, E_c^{nl}, which is calculated using a double space integral of the form

$$E_c^{nl} = \iint d\mathbf{r}_1 \, d\mathbf{r}_2 \, n(\mathbf{r}_1)\varphi(\mathbf{r}_1, \mathbf{r}_2)n(\mathbf{r}_2) \qquad (6)$$

where $n(\mathbf{r})$ is the electron density and φ is an integration kernel. The choice of exchange functional is important, as the original vdW-DF approach was shown to produce intermolecular binding distances that were too large.[9] The optPBE functional seeks to overcome these problems by using a less repulsive exchange functional.[9]

Energetics. All possible adsorption sites on the surface of the NPs are grouped into a series of symmetry-inequivalent sites. The sites for both cluster geometries are shown in Figure 1. On the 38-atom TO, which possesses both (111) and (100)
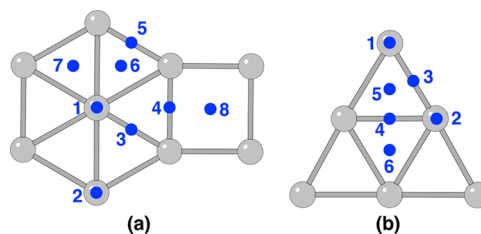

Figure 1. Symmetry-inequivalent CO adsorption sites for the 38-atom TO (a) and 55-atom Ico (b).

facets, 1 and 2 are atop sites, 3, 4, and 5 are bridge sites, and 6, 7, and 8 are hollow sites. On the 55-atom Ico 1 and 2 are atop sites, 3 and 4 are bridge sites, and 5 and 6 are hollow sites. Calculations are performed by placing a single CO molecule at each of these sites and performing a local minimization with VASP.

The energy of the chemisorption of CO onto a metal cluster is defined as

$$E_{ads} = E_{clus+CO} - E_{clus} - E_{CO} \qquad (7)$$

where $E_{clus+CO}$, E_{clus}, and E_{CO} are the energies of the cluster doped with CO, the bare cluster, and the CO molecule. A more negative E_{ads} represents a more strongly bound CO molecule.

Relative energies are defined as the difference between the energy of a particular locally minimized site E and that of the lowest energy site E_{min} for each functional

$$\Delta E_{ads} = E_{min} - E \qquad (8)$$

■ RESULTS AND DISCUSSION

The average M−M and C−O bond lengths for Pt, Au, Pd, and Ir clusters are given in Tables 1, 2, 3, and 4, respectively. For TO$_{38}$ the average M−M bond length decreases slightly for both D2 and D3 functionals. The optPBE functional shows a slight increase for all metals but Pt. The choice of functional typically has very little effect on the C−O bond length with the largest variation seen for the D2 functional.

Similarly, for Ico$_{55}$ the average M−M bond length decreases slightly for both D2 and D3 functionals with the optPBE functional showing a slight increase. There is more variation seen in the C−O bond length for Pt and Au with largest variation shown for optPBE.

Platinum. The adsorption energies, lowest energy sites, and average bond lengths for each functional are shown in Table 1. The relative energies for the symmetry-inequivalent sites are given in Figure 2.

The magnitude of E_{ads} can vary by as much as 0.5 eV on the TO structure with a maximum and minimum given by the D2 correction and the optPBE functional, respectively. There is less variation on the Ico structure.

On the 38-atom TO the PBE, D3 and optPBE functionals all show CO to favor site 4, a bridge site between the (111) and (100) facets, and predict similar barriers between the various sites. D3 shows higher energy differences for sites 6, 7, and 8 due to incomplete migration, where the CO molecule begins to move toward a new site and becomes trapped in a high energy

Table 1. Lowest and Highest Energy Sites, Absorption Energies E_{ads}, C−O Bond Lengths, Average M−M Bond Lengths, and M−M Bond Lengths as a Percentage of the Bulk %$_{Bulk}$ for the Pt 38-atom TO and 55-atom Ico

structure	xc	site$_{min}$	site$_{max}$	E_{ads}/eV	C−O/Å	M−M/Å	%$_{Bulk}$
TO	PBE	4	5	−2.248	1.180	2.701	68.92
	DFT+D2	3	5	−2.562	1.182	2.657	67.77
	DFT+D3	4	7	−2.407	1.182	2.704	68.99
	optPBE	4	5	−2.092	1.181	2.696	68.77
Ico	PBE	2	4	−2.458	1.162	2.758	70.36
	DFT+D2	1	6	−2.372	1.165	2.712	69.17
	DFT+D3	3	6	−2.463	1.183	2.742	69.94
	optPBE	3	6	−2.209	1.186	2.771	70.68

Table 2. Lowest and Highest Energy Sites, Absorption Energies E_{ads}, C−O Bond Lengths, Average M−M Bond Lengths, and M−M Bond Lengths as a Percentage of the Bulk %$_{Bulk}$ for the Au 38-atom TO and 55-atom Ico[a]

structure	xc	site$_{min}$	site$_{max}$	E_{ads}/eV	C−O/Å	M−M/Å	%$_{Bulk}$
TO	PBE	4	1	−0.990	1.180	2.827	69.30
	DFT+D2	8(4)	5	−1.439	1.179	2.774	68.00
	DFT+D3	3	1	−1.409	1.183	2.801	68.66
	optPBE	4	1	−0.874	1.180	2.839	69.59
Ico	PBE	4	2	−1.083	1.176	2.876	70.50
	DFT+D2	3	2	−2.687	1.176	2.818	69.07
	DFT+D3	5	3	−1.337	1.178	2.865	70.23
	optPBE	5	3	−1.089	1.157	2.888	70.78

[a]Site migrations are shown in brackets.

Table 3. Lowest and Highest Energy Sites, Absorption Energies E_{ads}, C−O Bond Lengths, Average M−M Bond Lengths, and M−M Bond Lengths as a Percentage of the Bulk %$_{Bulk}$ for the Pd 38-atom TO and 55-atom Ico

structure	xc	site$_{min}$	site$_{max}$	E_{ads}/eV	C−O/Å	M−M/Å	%$_{Bulk}$
TO	PBE	6	1	−2.115	1.197	2.727	70.09
	DFT+D2	6	1	−2.324	1.202	2.713	69.74
	DFT+D3	6	1	−2.249	1.196	2.713	69.73
	optPBE	6	1	−1.970	1.198	2.736	70.33
Ico	PBE	5	2	−2.279	1.201	2.759	70.91
	DFT+D2	5	1	−2.499	1.199	2.748	70.65
	DFT+D3	5	4	−2.459	1.202	2.742	70.49
	optPBE	5	2	−2.079	1.194	2.693	69.22

Table 4. Lowest and Highest Energy Sites, Absorption Energies E_{ads}, C−O Bond Lengths, Average M−M Bond Lengths, and M−M Bond Lengths as a Percentage of the Bulk %$_{Bulk}$ for the Ir 38-atom TO and 55-atom Ico

structure	xc	site$_{min}$	site$_{max}$	E_{ads}/eV	C−O/Å	M−M/Å	%$_{Bulk}$
TO	PBE	2	7	−2.529	1.171	2.646	68.91
	DFT+D2	2	6	−2.711	1.168	2.619	68.20
	DFT+D3	2	7	−2.632	1.170	2.638	68.70
	optPBE	2	6	−2.396	1.173	2.661	69.29
Ico	PBE	2	1	−2.843	1.168	2.678	69.75
	DFT+D2	2	3	−3.084	1.169	2.643	68.82
	DFT+D3	2	3	−2.932	1.169	2.668	69.47
	optPBE	2	3	−2.746	1.170	2.693	70.12

intermediate state. D2 displays different behavior to the other functionals, with the lowest energy site switching to site 3 and differences in the energetic ordering of the sites, as shown in Figure 3. Some significant cluster distortion is seen with the D2 functional, in particular the central atom of the (111) face is drawn out. Site 6 is also lower in energy after CO migrates to site 3. Overall the inclusion of D2 switches the preference of CO from the (111) to the (100) bridge site and appears to overestimate the effect of dispersion on the Pt-CO system.

The lowest energy site on the Ico varies with the choice of dispersion correction with site 2 preferred for PBE, site 1 for D2, and site 3 for D3 and optPBE. Site 1 and 2 are both atop sites and are favored by each functional, however, as the accuracy of the correction increases site 3, a bridge site, becomes competitive and eventually the lowest energy site. The same is true for site 4, another bridge site, whose energetic barrier decreases with the "accuracy" of the functional.

Overall the choice of correction can have a large effect on the properties of the Pt clusters. On the TO D2 appears to predict a site ordering too divergent to those predicted by the other functionals, whereas the higher accuracy D3 appears to trap CO in high energy intermediate sites. The optPBE vdW-DF then
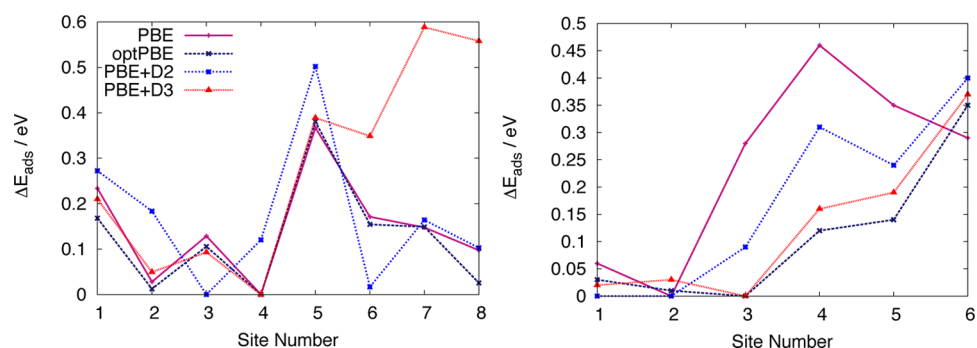
Figure 2. Relative energies ΔE_{ads} between the inequivalent binding sites of the Pt TO (left) and Ico (right) for each functional.
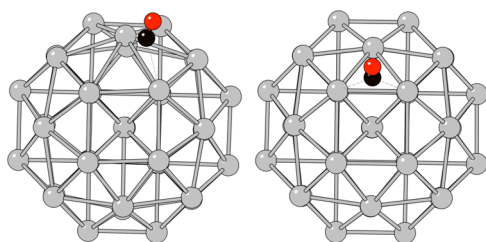

Figure 3. Lowest energy sites for the D2 functional (left) and all other functionals (right) for the Pt 38-atom TO.

gives an ordering very similar to the PBE functional and may mean that the inclusion of a dispersion correction is not necessary for the TO.

It appears, however, that the inclusion of dispersion for the Ico is necessary. As the "accuracy" of the functional is increased, there is no significant change in ordering but a successive decrease in the energetic barriers to sites 3, 4, and 5.

Gold. The adsorption energies, lowest energy sites, and average bond lengths for each functional are shown in Table 2. The relative energies for the symmetry-inequivalent sites are also given in Figure 4.

Similar to Pt, the different dispersion corrections can change E_{ads} by as much as 0.5 eV on the TO and 1.6 eV on the Ico. This large value for the Ico is due to a structural distortion of the structure which is discussed below.

Each functional seems to produce a different behavior in the Au TO. The PBE and optPBE functionals show the same preferences for site 4, a (100) bridge site, and both give a similar energetic ordering of sites. The optPBE functional predicts slightly higher energetic differences between sites when compared to PBE. Grimme's D2 and D3 corrections both show a similar energetic ordering, different to the PBE and optPBE
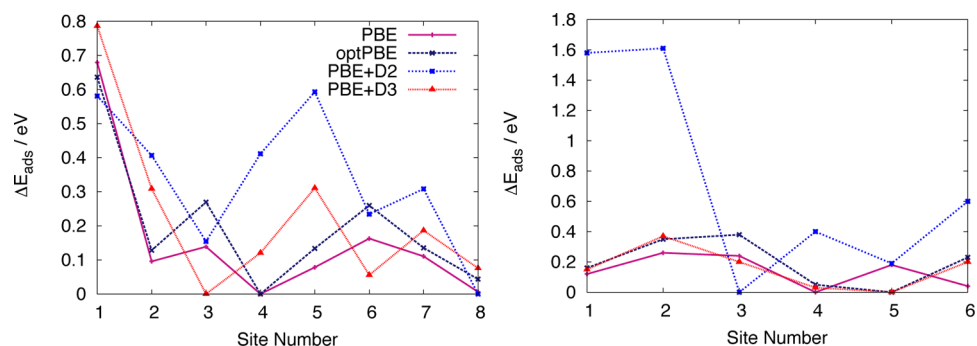
functionals with both possibly overestimating the effect of dispersion in the system. D3 predicts site 3 on the (111) face as the lowest energy site. The lowest energy site for D2 is site 8, where during the local minimization of the structure the CO has migrated to site 4, a bridge site between the (111) and (100) facets. The D2 functional causes significant distortion in the Au TO and this migration is followed by significant distortion of the cluster, as shown in Figure 5.
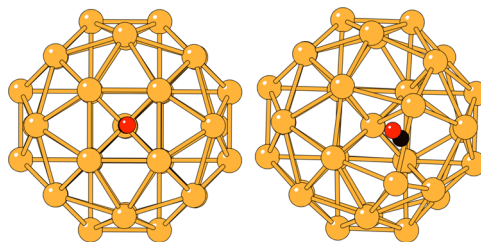

Figure 5. Initial (left) and final (right) structures for CO adsorption on site 8 of the Au TO. Significant distortion is seen in the final structure after local minimization with the D2 correction.

For the Ico structure, the D2 functional gives Au an energetic ordering of sites different to that of the other corrections with much larger energetic differences between sites. D2 causes significant distortion of the Ico when CO is adsorbed at sites 3, 4, and 5 and predicts the atop sites 1 and 2 to be particularly high in energy. This distortion accounts for the large binding energy for D2 shown in Table 2. D3 and optPBE both predict site 5 as the lowest energy site, with site 4 being highly competitive. At site 5, CO undergoes migration to site 4 for D3 and to site 1 for optPBE, adding further complication. Without any correction, site 4 is the lowest energy and is competitive for both D3 and optPBE.

Figure 4. Relative energies ΔE_{ads} between the inequivalent binding sites of the Au TO (left) and Ico (right) for each functional.

The inclusion of the D2 functional for either structure has a detrimental effect on their CO adsorption properties. Both Figures 5 and 6 show the significant distortion in the cluster
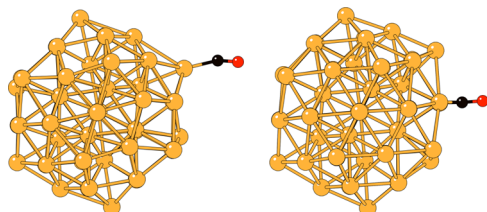

Figure 6. Au Ico structures from local minimization after CO adsorption at site 5 for D2 (left) and D3 (right). Both show the preference of CO to migrate to either site 1 or 4 and the significant distortion of the 55-atom Ico with the D2 functional.

geometry caused by the choice of the D2 functional. The effect of dispersion on the properties of Au may be best replicated by the higher accuracy functionals.

Palladium. The adsorption energies, lowest energy sites, and average bond lengths for each functional are shown in Table 3. The relative energies for the symmetry-inequivalent sites are also given in Figure 7. The lowest energy structures are shown in Figure 8

The dispersion corrections have only a minor effect on the Pd TO. Each functional predicts site 6, a hollow, as the lowest energy site and site 5 as highly competitive. There are no overall changes in energetic ordering and only subtle differences in the relative energies. The magnitude of E_{ads}, however, still varies with dispersion correction. Particularly large variations are seen for the Ico structure.

For the Ico structure all functionals predict site 5, another hollow site, as the lowest energy site. All functionals show a similar energetic ordering, with a some larger differences for D2 and D3 seen at site 4, a bridge site. No site migration is seen at site 5, differing from the other metals which normally favor migration to either site 1 or site 4.

Iridium. The adsorption energies, lowest energy sites, and average bond lengths for each functional are shown in Table 3. The relative energies for the symmetry-inequivalent sites are also given in Figure 9.

On both structures the lowest energy adsorption sites are atop, as shown in Figure 10. No significant quantitative differences are seen between the various dispersion corrections for the Ir TO. Some differences that are seen are the smaller energetic difference for site 6 predicted by D3 and higher
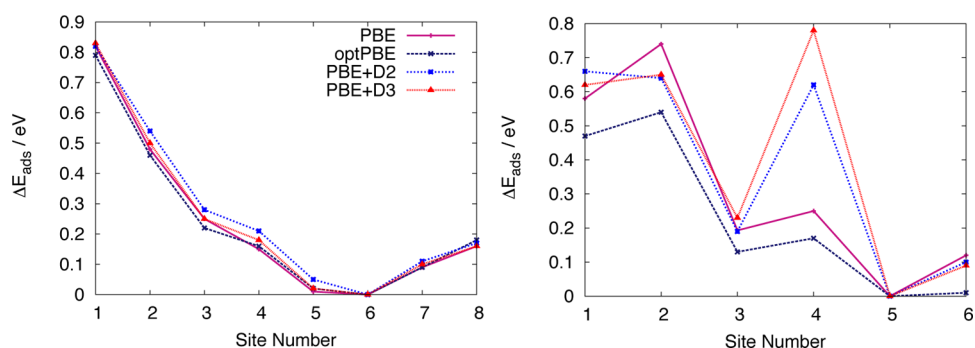
energetic difference for site 8 predicted by optPBE. Some more subtle differences are seen, for example, between sites 1 and 2.

The three hollow sites, 6, 7, and 8, are all strongly disfavored. At site 6 all but D3 favor migration to the bridge site 3, at site 7 all functionals predict migration to site 3, and at site 8 all functionals predict migration to bridge site 4 except optPBE where no migration occurs.

Similar to the TO, the inclusion of dispersion at any level of theory has no great effect on the Ir Ico cluster. Each functional predicts a preference for atop site 2, shown in Figure 10. Again hollow sites are found to be disfavored. Site 5 is particularly sensitive and each functional predicts CO to migrate to bridge site 4. Site 6 is less sensitive, with migration occurring for PBE, slight migration for D2 and D3 and complete migration for optPBE. This is shown by the range of relative energies shown in Figure 9.

Figure 8. Energetically preferred sites for Pd TO$_{38}$ (left) and Ico$_{55}$ (right) for all functionals.

■ CONCLUSIONS AND FUTURE WORK

The decision as to whether a dispersion correction should be included in an adsorption study on a metal cluster is complex. The site preference for CO is shown to depend on the metal, the functional, and the geometry of the cluster. It appears that the effect of dispersion correction can be subtle, as when applied to the Ir TO and Ico NPs, or have large effects on the underlying nanoparticle structure, as with the Au NPs. The effect of the functionals on the Pt NPs is more nuanced and shows the importance of considering a dispersion functional when studying its catalytic properties.

The PBE+D2 correction, the simplest considered, is found to give results that are qualitatively different from those of the other dispersion corrections and PBE functionals. The higher accuracy corrections tend to give similar results to one another. This, however, is not a clear indication as to whether a dispersion correction is necessary.

Figure 7. Relative energies ΔE_{ads} between the inequivalent binding sites of the Pd TO (left) and Ico (right) for each functional.
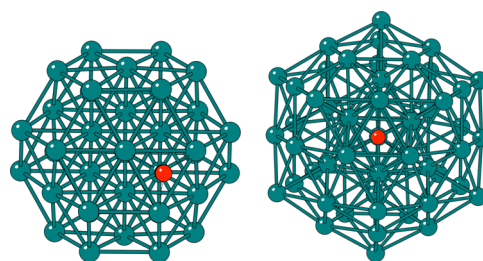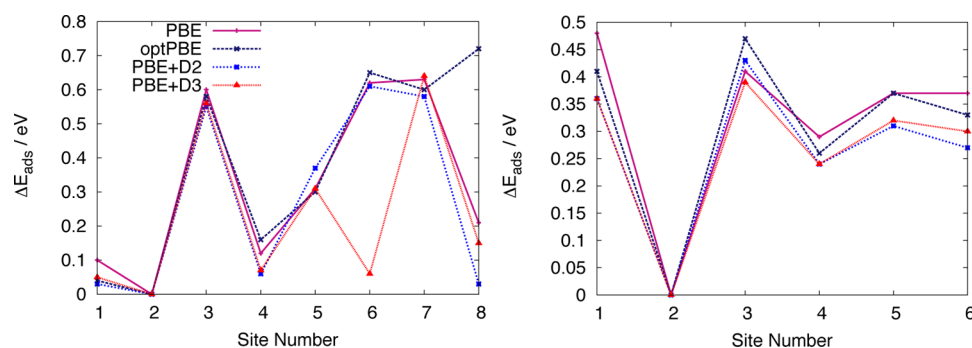
Figure 9. Relative energies ΔE_{ads} between the inequivalent binding sites of the Ir TO (left) and Ico (right) for each functional.
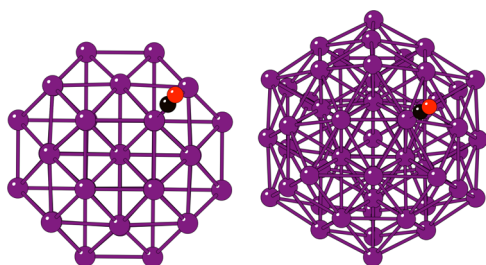

Figure 10. Lowest energy CO binding site for TO$_{38}$ (left) and Ico$_{55}$ (right) for all functionals.

The D2 and optPBE dispersion corrections both lack many-body terms. These have shown to be essential in the accurate description of dispersion interactions in a variety of systems and may be particularly relevant in our systems.[10,11] Only the D3 correction contains three-body terms and, therefore, in some cases may yield a more accurate result.

Future work will include the application of dispersion corrected methods that include these many-body interactions. This will allow the accurate modeling of a variety of catalytically relevant reactions and will involve the direct comparison to experimental results.

■ AUTHOR INFORMATION

Corresponding Author
*E-mail: r.l.johnston@bham.ac.uk.

Notes
The authors declare no competing financial interest.

■ ACKNOWLEDGMENTS

■ REFERENCES

(1) Hohenberg, P.; Kohn, W. Inhomogeneous Electron Gas. *Phys. Rev.* **1964**, *136*, 864−871.

(2) Kohn, W.; Sham, L. J. Self-Consistent Equations Including Exchange and Correlations Effects. *Phys. Rev.* **1965**, *140*, 1133−1138.

(3) Grimme, S. Semiempirical GGA-Type Density Functional Constructed with a Long-Range Dispersion Correction. *J. Comput. Chem.* **2006**, *27*, 1787−1799.

(4) Grimme, S. Accurate Description of Van der Waals Complexes by Density Functional Theory Including Empirical Corrections. *J. Comput. Chem.* **2004**, *25*, 1463−1473.

(5) Grimme, S.; Antony, J.; Ehrlich, S.; Krieg, H. A Consistent and Accurate Ab Initio Parametrization of Density Functional Dispersion Correction (DFT-D) for the 94 Elements H-Pu. *J. Chem. Phys.* **2010**, *132*, 154104.

(6) Dion, M.; Rydberg, H.; Schröder, E.; Langreth, D. C.; Lundqvist, B. I. Van der Waals Density Functional for General Geometries. *Phys. Rev. Lett.* **2004**, *92*, 246401.

(7) Lee, K.; Murray, E. D.; Kong, L.; Lundqvist, B. I.; Langreth, D. C. Higher-accuracy Van der Waals Density Functional. *Phys. Rev. B: Condens. Matter Mater. Phys.* **2010**, *82*, 081101.

(8) Klimeš, J.; Bowler, D. R.; Michaelides, A. Chemical Accuracy for the Van der Waals Density Functional. *J. Phys.: Condens. Matter* **2010**, *22*, 022201.

(9) Klimeš, J.; Bowler, D. R.; Michaelides, A. Van der Waals Density Functionals Applied to Solids. *Phys. Rev. B: Condens. Matter Mater. Phys.* **2011**, *83*, 195131.

(10) Tkatchenko, A. Current Understanding of Van der Waals Effects in Realistic Materials. *Adv. Funct. Mater.* **2015**, *25*, 2054−2061.

(11) Kronik, L.; Tkatchenko, A. Understanding Molecular Crystals with Dispersion-Inclusive Density Functional Theory: Pairwise Corrections and Beyond. *Acc. Chem. Res.* **2014**, *47*, 3208−3216.

(12) Klimeš, J.; Michaelides, A. Perspective: Advances and Challenges in Treating Van der Waals Dispersion Forces in Density Dunctional Theory. *J. Chem. Phys.* **2012**, *137*, 120901.

(13) Dobson, J. F.; White, A.; Rubio, A. Asymptotics of the Dispersion Interaction: Analytic Benchmarks for Van der Waals Energy Functionals. *Phys. Rev. Lett.* **2006**, *96*, 073201.

(14) Tkatchenko, A.; Scheffler, M. Accurate Molecular Van Der Waals Interactions from Ground-State Electron Density and Free-Atom Reference Data. *Phys. Rev. Lett.* **2009**, *102*, 073005.

(15) Becke, A. D.; Johnson, E. R. A Simple Effective Potential for Exchange. *J. Chem. Phys.* **2006**, *124*, 221101.

(16) Bloński, P.; López, N. On the Adsorption of Formaldehyde and Methanol on a Water-Covered Pt(111): A DFT-D Study. *J. Phys. Chem. C* **2012**, *116*, 15484−15492.

(17) Pereira, A. O.; Miranda, C. R. Atomic Scale Insights Into Ethanol Oxidation on Pt, Pd and Au Metallic Nanofilms: A DFT with Van der Waals Interactions. *Appl. Surf. Sci.* **2014**, *288*, 564−571.

(18) Chwee, T. S.; Sullivan, M. B. Adsorption Studies of C6H6 on Cu (111), Ag (111), and Au (111) within Dispersion Corrected Density Functional Theory. *J. Chem. Phys.* **2012**, *137*, 134703.

(19) Tereshchuk, P.; Da Silva, J. L. F. Ethanol and Water Adsorption on Close-Packed 3d, 4d, and 5d Transition-Metal Surfaces: a Density Functional Theory Investigation with Van der Waals Correction. *J. Phys. Chem. C* **2012**, *116*, 24695−24705.

(20) Feibelman, P. J.; Hammer, B.; Norskov, J. K.; Wagner, F.; Scheffler, M.; Stumpf, R.; Watwe, R.; Dumesic, J. The CO/Pt (111) Puzzle. *J. Phys. Chem. B* **2001**, *105*, 4018−4025.

(21) Alaei, M.; Akbarzadeh, H.; Gholizadeh, H.; de Gironcoli, S. CO/Pt(111): GGA Density Functional Study of Site Preference for Adsorption. *Phys. Rev. B: Condens. Matter Mater. Phys.* **2008**, *77*, 085414.

(22) Stroppa, A.; Kresse, G. The Shortcomings of Semi-Local and Hybrid Functionals: What We Can Learn from Surface Science Studies. *New J. Phys.* **2008**, *10*, 063020.

(23) Lazić, P.; Alaei, M.; Atodiresei, N.; Caciuc, V.; Brako, R.; Blügel, S. Density Functional Theory with Nonlocal Correlation: A Key to the Solution of the CO Adsorption Puzzle. *Phys. Rev. B: Condens. Matter Mater. Phys.* **2010**, *81*, 045401.

(24) Kerpal, C.; Harding, D. J.; Meijer, G.; Fielicke, A. CO Adsorption on Neutral Iridium Clusters. *Eur. Phys. J. D* **2011**, *63*, 231−234.

(25) Remediakis, I. N.; Lopez, N.; Nørskov, J. K. CO Oxidation on Gold Nanoparticles: Theoretical Studies. *Appl. Catal., A* **2005**, *291*, 13−20.

(26) Yudanov, I. V.; Sahnoun, R.; Neyman, K. M.; Rosch, N.; Hoffmann, J.; Schauermann, S.; Johanek, V.; Unterhalt, H.; Rupprechter, G.; Libuba, J.; et al. CO Adsorption on Pd Nanoparticles: Density Functional and Vibrational Spectroscopy Studies. *J. Phys. Chem. B* **2003**, *107*, 255−264.

(27) Liao, M.-S.; Cabrera, C. R.; Ishikawa, Y. A Theoretical Study of CO Adsorption on Pt, Ru and Pt-M (M= Ru, Sn, Ge) Clusters. *Surf. Sci.* **2000**, *445*, 267−282.

(28) Davis, J. B. A.; Horswell, S. L.; Piccolo, L.; Johnston, R. L. Computational Study of the Adsorption of Benzene and Hydrogen on Palladium-Iridium Nanoalloys. *J. Organomet. Chem.* **2015**, *792*, 190−193.

(29) Kresse, G.; Hafner, J. Ab Initio Molecular-Dynamics Simulation of the Liquid-Metal-Amorphous-Semiconductor Transition in Germanium. *Phys. Rev. B: Condens. Matter Mater. Phys.* **1994**, *49*, 14251−14269.

(30) Kresse, G.; Hafner, J. Ab initio molecular Dynamics for Liquid Metals. *Phys. Rev. B: Condens. Matter Mater. Phys.* **1993**, *47*, 558−561.

(31) Kresse, G.; Furthmüller, J. Efficiency of Ab-Initio Total Energy Calculations for Metals and Semiconductors Using a Plane-Wave Basis Set. *Comput. Mater. Sci.* **1996**, *6*, 15−50.

(32) Kresse, G.; Furthmüller, J. Efficient Iterative Schemes for Ab Initio Total-Energy Calculations using a Plane-Wave Basis Set. *Phys. Rev. B: Condens. Matter Mater. Phys.* **1996**, *54*, 11169−11186.

(33) Methfessel, M.; Paxton, A. T. High-Precision Sampling for Brillouin-Zone Integration in Metals. *Phys. Rev. B: Condens. Matter Mater. Phys.* **1989**, *40*, 3616−3621.

(34) Perdew, J.; Burke, K.; Wang, Y. Generalized Gradient Approximation for the Exchange-Correlation Hole of a Many-Electron System. *Phys. Rev. B: Condens. Matter Mater. Phys.* **1996**, *54*, 533−539.